Fast Finite-Difference Modeling of 3-D Elastic Wave Propagation

S 23.7

Rune Mittet, Continental Shelf and Petroleum Technology Research Institute A/S (IKU);
Olav Holberg, Informasjonskontroll A/S; Borge Arntsen and Lasse Amundsen, IKU, Norway

Summary

We present an efficient method for wavefield modeling in arbitrarily inhomogeneous 3-D elastic media, based on optimized difference operators for spatial differentiation (Holberg, 1987). This technique offers accurate results on coarse spatial grids, ie. of the order of 3 gridpoints per shortest wavelength. In 3-D applications, this fast finite difference technique is at least two orders of magnitude more efficient than conventional finite difference schemes and typically 2.5 to 6 times more efficient than the pseudospectral method, depending on the sampling of the model. This makes it practicable to run realistic 3-D simulations on existing vector computers. In the present paper we discuss the practical implementation of this method and give timings for various model sizes and computer configurations. We also give several numerical examples, ranging from simulations in simple geometries with well known solutions to geometries of realistic complexity.

Introduction

Efficient numerical simulation of elastic wave propagation in complex geological media is of considerable importance in exploration and production seismology. Modeling is often used to study amplitude variations with offset in areas with strong lateral velocity gradients and to study diffractions from fault zones and converted shear waves from deep complex structures. Particularly, accurate 3-D elastic modeling capability is becoming increasingly important as we collect more 3-D data and search for smaller and more complex reservoirs. Also, proper numerical modeling will find applications in future modeling-driven seismic inversion schemes. All these factors pose stringent requirements on the modeling algorithm.

Direct numerical techniques, like finite differencing, handle any kind of waves in arbitrarily inhomogeneous media. However, conventional finite difference schemes require a gross oversampling of the model to produce accurate results. For this reason finite difference techniques have not yet been applicable to models of realistic size. This heavy oversampling of the model is now obsolete. By using properly designed difference operators for spatial differentiation (Holberg, 1987), one can obtain excellent results with order of 3 grid point per shortest wavelength when the differentiator half-length is 4 to 6 samples. In 3-D modeling, this capability reduces the requirements for computer time and storage by more than two orders of magnitude.

In the present work we have used this powerful fast finite difference technique to realize efficient 3-D elastic modeling. We solve the elastodynamic equations for the stresses and use a staggered grid formulation similar to the one used by Virieux (1986). By calculating different field quantities on different sets of gridpoints we avoid the use of inaccurate centered derivative operators. By using a stress formulation, the free surface boundary conditions are easily modeled. Also, the resulting scheme is then stable for all values of Poisson's ratio and liquid-solid interfaces are handled accurately without the need to explicitly specify the boundary conditions at such interfaces (Levander, 1987).

Implementation

We let i, j and k represent the directions in a right handed coordinate system (ie. a cyclic permutation of x, y and z). The corresponding integer coordinates are I, J and K, hence $x_k = (K-1)\Delta x_k$. The equation for a diagonal stress component is then

$$\partial_t^2 \sigma_{ii}(I,J,K,t) = [\lambda(I,J,K) + 2\mu(I,J,K)]\,\partial_i^- A_i(I+\tfrac{1}{2},J,K,t) + \lambda(I,J,K)\left[\partial_j^- A_j(I,J+\tfrac{1}{2},K,t) + \partial_k^- A_k(I,J,K+\tfrac{1}{2},t)\right] \quad (1)$$

and the equation for a shear stress component is

$$\partial_t^2 \sigma_{ik}\left(I+\tfrac{1}{2},J,K+\tfrac{1}{2},t\right) = \mu\left(I+\tfrac{1}{2},J,K+\tfrac{1}{2}\right)\left[\partial_k^+ A_i(I+\tfrac{1}{2},J,K,t) + \partial_i^+ A_k(I,J,K+\tfrac{1}{2},t)\right] \quad (2)$$

A component of the acceleration, A_j, is defined as

$$A_j(I,J+\tfrac{1}{2},K,t) = \rho^{-1}(I,J+\tfrac{1}{2},K)\left[\partial_j^+ \sigma_{jj}(I,J,K,t) + \partial_i^- \sigma_{ij}(I+\tfrac{1}{2},J+\tfrac{1}{2},K,t) + \partial_k^- \sigma_{jk}(I,J+\tfrac{1}{2},K+\tfrac{1}{2},t) + f_j(I,J+\tfrac{1}{2},k)g(t)\right] \quad (3)$$

Here ρ is the density and λ and μ are the two Lamé parameters. The forward (∂^+) and backward (∂^-) difference operators are defined in Holberg (1987). The source time function is $g(t)$ and f_j is the jth component of the spatial part of the source function.

To be able to describe a directional source or a P-wave source we introduce a bandlimited Dirac δ-function as

$$\tilde{\delta}(x_j - x_j^s) = \lim_{k \to k_m} \frac{1}{\sqrt{\pi}} k_m e^{-k_m^2 (x_j - x_j^s)^2} \quad (4)$$

and adjust the spatial bandwith, using k_m, so that the source is approximately pointlike. This is easily obtained for a directional source, since it can be represented as a force on a single mesh point. A pressure source, however, has a more complicated spatial dependence and behaves as a sum of dipole contributions and must be spread out over 6 or more meshpoints in 3-D pseudospectral or finite difference calculations.

We use standard second order temporal differencing of the stress fields. All calculations are performed on $x-y$ planes of field-values. For each recursive time step the algorithm steps the $x-y$ planes of computation down through the complete spatial data volume. To solve the puzzle of minimizing the memory requirements while optimizing the numerical operations and not creating additional I/O, we store in memory the relevant fields and sums of spatial derivatives of the fields in slabs of thickness ranging from 2 up to $2L_z+1$, where L_z is the differentiator half-length in the z-direction.

Numerical examples

To demonstrate the accuracy of our method for a coarse grid, we compare our finite difference solution with the solution to Lamb's problem for a P-wave source calculated with a reflectivity algorithm. The result is shown in Figure 1. The source and receiver locations together with densities, P-wave velocities and S-wave velocities for the two media are given in Figure 1a. In Figure 1b to 1g the solid line is the finite difference solution whereas the reflectivity solution is plotted with a dashed line.

The events, in order of increasing time, are the direct P-wave, the P-wave to P-wave reflection and the P-wave to S-wave reflection. This calculation is performed with 3.0 gridpoints per shortest wavelength in space and we find excellent agreement between the two methods at all offsets. Preliminary results indicate that we must expect some amplitude deviations at large offsets if the number of gridpoints per shortest wavelength is reduced towards 2.0.

We have performed a full-scale simulation of 4 seconds of data for the model shown in Figure 2. This model is 3.3 km × 2.2 km × 2.8 km in the x, y and z directions respectively. The source bandwith is 30 Hz and the grid spacing is 17.5 meters. The explosive source, marked with a star in Figure 2, is located in the water layer 8.75 meters below a free surface. In the underlying solid layers, the density and P-wave and S-wave velocities increase with depth from 1.87 g/cm^3, 1995 m/s and 1220 m/s in layer II to 2.48 g/cm^3, 3490 m/s and 2400 m/s in layer IX. The exceptions being a reduction in S-wave velocity in layer IV and low P-wave and S-wave velocities in layer VII compared to the neighbouring layers (ie. 2415 m/s and 1195 m/s).

Our algorithm allows snapshots to be recorded in several cross sections normal to any of the three axis, x, y or z and at a number of offsets and/or depths. For the snapshots, we display the pressure field $P = -\frac{1}{3}(\sigma_{xx} + \sigma_{yy} + \sigma_{zz})$ and we calculate the curl of the acceleration field to have a picture of the rotational motion in the medium. The reason for using the acceleration as the basis for the shear-wave snapshots is that it is readily available from the calculations as a sum of derivatives of stress fields and requires little preparation before display. The price to pay for this is that the fields we display show several rapid oscillations. This is not due to any dispersion effects but to the fact that the components of curl$\vec{A}$ are formally obtained by several temporal and spatial differentiations of the displacement field.

For simple geometrical models we find that the recorded P-wave and S-wave fields have several spatial symmetries, which make them easy to interpret. As we increase the 3-D complications, the recorded fields grow progressively more complicated and irregular as is clearly seen in both Figure 3 and 4 which display snapshots in a plane normal to the z-axis at a depth of 1.7 km. In general there will be P-waves, S-waves and surface waves travelling in the snapshot planes and in a number of directions through these planes. For this reason, it is essential to be able to record several snapshots normal to all three axis in a complicated 3-D geometry to perform a satisfactory interpretation of the main events. In the first snapshot in Figure 3 we see the downgoing P-wave passing through the snapshot plane. The complexity of the model causes the deviations from a perfect circle for the downgoing P-wave. Consecutive snapshots show how the direct P-wave and reflected and converted P-waves evolves in time. The inner circle on the last snapshot in Figure 3 is the first surface multiple propagating through the snapshot plane, interfering locally with other wave phenomena. The initial shear wave snapshot in Figure 4 consists of energy which has propagated most of the way as P-waves before conversions to S-waves near the depth of the snapshot plane. At later times we see how several S-wave modes are excited or arrive at this depth and create complicated wave patterns.

For the shot-gathers and vertical seismic profiles we extract from the calculation the pressure field and the three components of particle velocities, v_x, v_y and v_z. In Figure 5 we show a complete VSP recording from the numerical experiment performed in the model shown in Figure 2. The VSP recording is 1 km offset from the source and marked with the thick solid line in Figure 2. It is interesting to note that the v_z waves are transmitted through the elastic/acoustic interface at the top of the model and hence appear as continous over the interface, whereas upgoing v_x and v_y waves are more or less totally reflected at this interface. There are some small upgoing waves at the bottom of the VSP sections. This is due to the fact that we have not yet had the time to put any effort into the optimization of the the absorbing boundary conditions for our scheme.

Timings

This algorithm vectorizes easily and tests on a CRAY X-MP/28 with an SSD have shown that the scheme is CPU bound. For a coarse grid model of size 128 × 128 × 128 meshpoints, the elapsed wall clock time for completing 1000 time-steps was 102 minutes. We were utilizing a single processor on the CRAY X-MP/28 in this case. We can reduce the time of computation with a factor approaching 4 by multitasking the algorithm on a CRAY X-MP/48.

For the model shown in Figure 2 the elapsed time is approximately 8 hours utilizing a single processor on a CRAY X-MP/28.

Conclusions

The fast finite difference technique provides an accurate and efficient tool for modeling wave propagation in geologically complex media.

Seismograms calculated for Lamb's problem demonstrate excellent accuracy for relatively coarse grids, ie. 3.0 gridpoints per shortest wavelength. If the grid is further coarsened towards the Nyquist limit we find some inaccuracies in reflection amplitudes due to the coarse sampling of the model. However, it appears that this problem is inherent to all discrete methods and is not related to our differencing technique.

At 3.0 gridpoints per shortest wavelength the fast finite difference method is 6 times faster than the pseudospectral method and at least two orders of magnitude more efficient than second order finite difference schemes.

Acknowledgements

The authors wish to thank Esso Norge A/S for financial support. We are also grateful to J.R. Berryhill of Exxon Production Research Company for encouraging this work.

REFERENCES

M. Edwards, C. Hsiung, D. Kosloff and M. Reshef 1985, Elastic 3-D Forward Modeling by the Fourier Method, Presented at the 55th Annual Meeting of the Society of Exploration Geophysicists, Washington, DC.

O. Holberg 1987, Computational Aspects of the Choice of Operator and Sampling Interval for Numerical Differentiation in Large-Scale Simulations of Wave Phenomena, Geophysical Prospecting 35, 629 - 655.

A. R. Levander, 1987, Fourth-Order Velocity Stress Finite-Difference Scheme, Presented at the 57th Annual Meeting of the Society of Exploration Geophysicists, New Orleans.

J. Virieux, 1986, P-SV wave propagation in heterogeneous media: Velocity- stress finite-difference method, Geophysics 51, 889

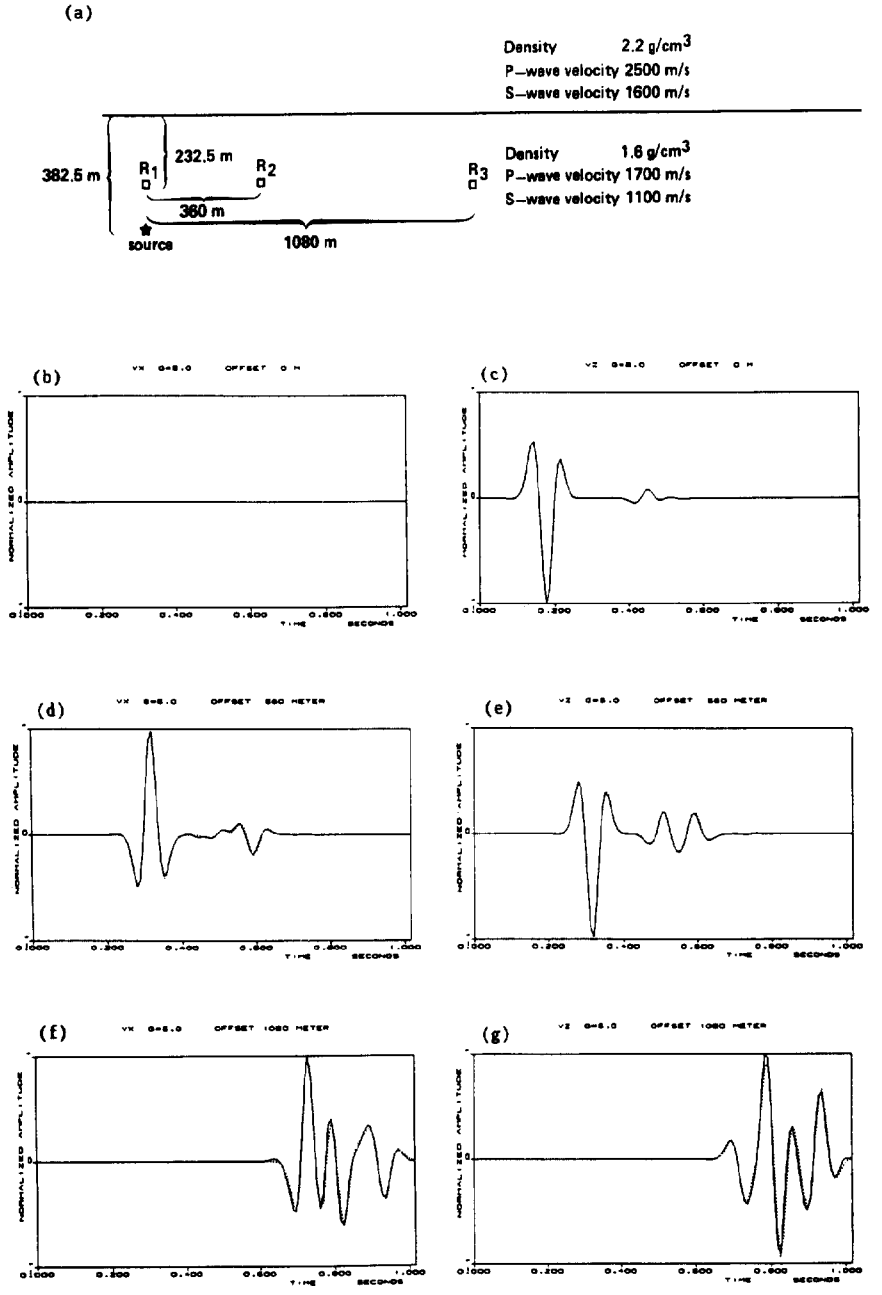

FIG. 1. Comparison of finite-difference and reflectivity methods.

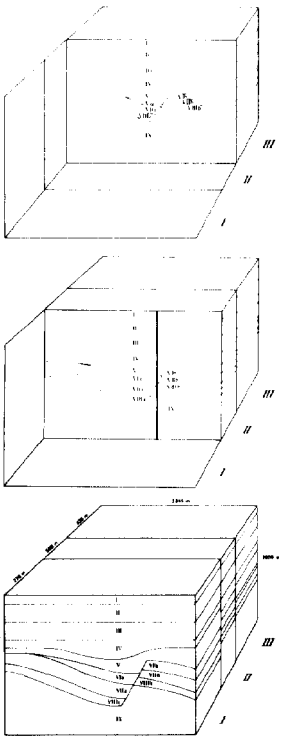

FIG. 2. 3-D model for numerical experiment.

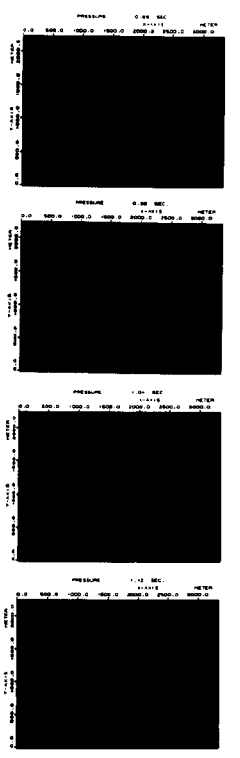

FIG. 3. *P*-wave snapshots.

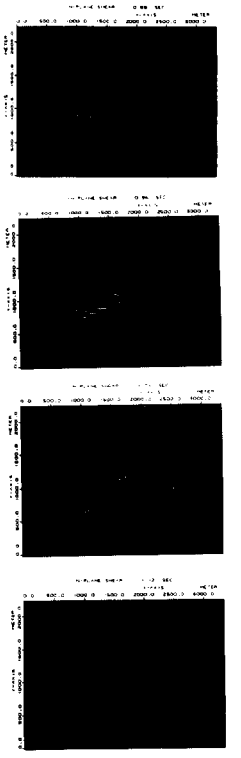

FIG. 4. In-plane *S*-wave snapshots.

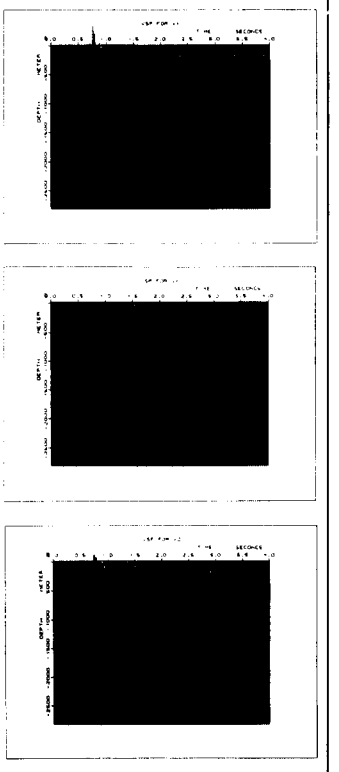

FIG. 5. VSP recording.